Plasma assisted catalytic decomposition of CO_2

Guoxing Chen [a,b,*], Violeta Georgieva [a], Thomas Godfroid [c], Rony Snyders [b,c], Marie-Paule Delplancke-Ogletree [a]

[a] 4MAT, Université Libre de Bruxelles, 50 Av. F.D. Roosevelt, 1050 Brussels, Belgium
[b] ChIPS, Université de Mons, 23 Place du Parc, 7000 Mons, Belgium
[c] Materia Nova Research Center, Av. N. Copernic 1, 7000 Mons, Belgium

A R T I C L E   I N F O

A B S T R A C T

In this research, conversion of carbon dioxide in the presence of TiO_2 supported NiO catalyst has been investigated in a pulsed surface-wave sustained microwave discharge. The catalyst is prepared by combination of impregnation and plasma-treatment methods. The decomposition of TiO_2 supported nickel nitrate was done by plasma, induced in three different gases (O_2, Ar, CO_2). NiO/TiO_2 catalysts were formed. The supplied gas has a prominent effect on the chemical and physical properties of the prepared catalysts. The catalyst prepared with an Ar plasma increases almost by a factor of 2 the CO_2 conversion and energy efficiencies, while the O_2 or CO_2 plasma prepared catalysts show little effect on the CO_2 conversion in comparison with catalyst-free plasma assisted dissociation. The results from the catalyst characterization by different techniques demonstrated that Ar plasma pre-treatment resulted in formation of oxygen vacancies. Dissociative electron attachment of CO_2 at the catalyst surface enhanced by oxygen vacancies and plasma electrons could explain the improved conversion and energy efficiency. A constant catalytic activity was observed indicating continuous catalyst regeneration under reactor conditions. A mechanism of plasma-catalysis synergy is proposed.

© 2016 Elsevier B.V. All rights reserved.

1. Introduction

The decrease of natural reserves of fossil fuels and the greenhouse effect from CO_2 emissions generated by anthropomorphic activities drives the search for new "green" sources of fuels. A promising solution is the usage of electrical energy produced, for example, by renewable or nuclear sources for dissociation of CO_2 or other greenhouse gases and their conversion into synthetic fuels which can be easily stored. In this context, the CO_2 re-utilization to synthesize syngas, fuels or chemical compounds as well as pure CO_2 dissociation into CO and O_2, attract a lot of attention.

Different techniques for conversion of CO_2 into value-added chemical compounds or fuels have been developed and studied, namely thermolysis, photocatalysis and electrochemical methods [1–8]. The thermal CO_2 splitting is thermodynamically and energetically favorable only at very high temperatures (1400–1800 °C) and the conversion efficiency is very low [1]. A membrane reactor system, such as calcium oxide zirconia membrane, may enhance

the process [2]. CO_2 conversion efficiency of 21.5% was reached at 1700 °C in thermal CO_2 dissociation which is considerably higher than the CO_2 conversion efficiency of 1.2% at the same temperature in pure thermal process [2]. Although photocatalytic conversion of CO_2 shows great potential at the present time by using solar energy, the drawbacks are the low CO_2 conversion efficiency (e.g. <1%), long periods of irradiation for the catalyst activation, and specific requirements for the bandgap energy of the catalyst [3–7]. High-temperature electrolysis seems to be promising considering the electric energy to liquid fuel energy conversion that reaches 78–87% [4,8]. However, it has disadvantages like using scarce or expensive materials, high operating temperature (800–1000 °C), heating of the whole system, large size of the system, and short durability of the electrodes. The energy efficiencies are defined in different ways for the thermal, photocatalytic and electrolytic CO_2 dissociation and cannot be compared directly. An alternative method to the techniques described above can be plasma or plasma-catalysis CO_2 dissociation since plasma can be easily sustained by a power source. In addition, as we discuss below, it is possible to use abundant, durable and not expensive materials for catalysts. In the past decade, non-thermal plasmas have been shown to be effective and efficient in activation of CO_2 [9–23]. Liu et al. [9] reviewed non-thermal plasma technologies for the utilization of carbon dioxide.

* Corresponding author at: Université Libre de Bruxelles, 50 Av. F.D. Roosevelt—CP165/63, 1050 Brussels, Belgium. Fax: +32 0 2650 2932.
E-mail addresses: guoxchen@ulb.ac.be, guoxing.chen@umons.ac.be (G. Chen).

Fridman [10] reviewed the plasma physics of CO_2 reduction to CO and its application. To synthesize fuel from CO_2, it is combined with a hydrogen-containing gas such as H_2 [24–26], CH_4 [27–33], or H_2O [34–37].

There have been several studies of plasma-assisted dissociation of pure CO_2 in the recent years [11–13]. Results are also reported for mixtures of CO_2 with an inert gas [14–23]. However, a trade-off between the energy and conversion efficiencies is observed in plasma processing. We propose plasma assisted catalytic process with plasma-activation of the catalysts to increase energy efficiency while maintaining high conversion rate. The combination of heterogeneous catalysis and plasma activation, known as plasma-catalysis, has attracted increasing interest [38,39]. On one hand, the catalyst can increase reaction rates and selectivity. On the other hand, the non-thermal plasma provides the energy to drive highly endothermic processes such as CO_2 dissociation. Plasma-catalytic processes have great potential to reduce the activation barrier of different reactions and improve the conversion rates. The non-thermal plasma itself can influence the acid-base nature of the supports, enhance the dispersion of the supported metals, and even adjust the microstructure of the metal nanoparticles and metal-support interface [9,38], and in this way change the catalyst properties. All these factors contribute in different ways to enhancing the energy efficiency of the plasma process as well as the catalyst stability, due to a synergy that occurs between the catalyst and the plasma [33]. Plasma-catalysis has been widely investigated for gaseous pollutant abatement [38,39] and dry reforming of methane [27,29,30,33]. For the latter application, significant attention has been given to supported Ni catalysts due to their low cost and wide availability. Most of these studies focused primarily on identifying plasma-catalytic chemical reactions to maximize process performance, while the dynamic plasma-catalyst interaction have received less attention.

Up to now, few studies have investigated the non-thermal plasma driven catalysis for the CO_2 decomposition [15,19]. Brock et al. [15] studied the catalytic effect of metallic coating on the decomposition of CO_2 in fan-type AC glow discharge plasma reactors, using a gas mixture of 2.5% CO_2 in He. They showed that a Rh coated reactor has the highest activity for the CO_2 decomposition compared to the reactors coated with Cu, Au, Pt, Pd and mixed rotor/stator systems (Rh/Au and Au/Rh). Spencer and Gallimore [19] experimentally investigated the conversion of CO_2 in an atmospheric pressure microwave plasma-catalytic system. The results showed that Rh/TiO_2 coating on a monolithic cordierite structure used as a catalyst actually caused a drop in conversion efficiency due to reverse reactions occurring on the surface. The use of plasma techniques in catalyst preparation, regeneration and catalytic reactions were already reviewed in several works [40–42]. However, the influence of the gases used for plasma pre-treatment of the catalyst has not been investigated.

To our knowledge, the decomposition of pure CO_2 in a surface-wave sustained microwave discharge combined with TiO_2 supported NiO catalysts has not been investigated previously. Microwave plasma has been proven to be the most efficient plasma for pure CO_2 dissociation [10,24]. In addition, the advantages of the microwave plasma for greenhouse gas dissociation compared to other types of discharges were discussed in our previous work dealing with the simultaneous plasma-assisted dissociation of CO_2 and H_2O [34]. In the present work, we use plasma pre-treatment as a replacement of the conventional calcination in the catalyst preparation process. The influence of three different discharges, i.e. O_2, Ar, or CO_2 discharge, on the CO_2 conversion and energy efficiencies is studied. The fresh catalysts treated in the plasma-catalytic reactor were characterized by X-ray diffraction (XRD) and Brunauer-Emmett-Teller (BET) methods, Transmission electron microscopy (TEM), Raman Spectroscopy, and Ultraviolet–visible

(UV–vis) spectroscopy. The interactions between plasma and catalyst as well as the possible mechanism for CO_2 decomposition on the catalyst surface and catalyst regeneration are reported.

2. Experimental

2.1. The microwave discharge reactor

The experimental setup for pulsed microwave plasma generation used in this work is shown in Fig. 1. The discharge is generated at 915 MHz in a double-walled quartz tube with a 14 mm inner diameter and 31 cm length, cooled by 5 °C oil flowing between the inner (quartz) and the outer (polycarbonate) tubes. The CO_2 or the other gases are injected from the top of the system. The flow rate is regulated by electronic mass flow controllers ranging between 0 and 3 standard liter per minute (slm). A reactor containing the catalyst is connected to the end of the plasma tube so that the catalyst is positioned at around 3 cm below the plasma tube end. The following operating parameters were used for all plasma-catalysis CO_2 dissociation experiments: pure CO_2 is supplied at flow rate of 2 slm, the mean input power is 1000W at a pulse frequency of 1.67 kHz, which corresponds to a specific energy input of 6.95 eV/molecule. The pressure in the post discharge is set to 1330 Pa (10 Torr). The whole system is surrounded by a grounded aluminium grid to prevent any leakage of microwave radiation into the outer space. Pulsed plasmas with pulse duration of 300 μs, and a period of 600 μs were used. The impedance of the waveguide can be adapted by an automatic three stubs system in order to minimize the reflected microwave power. With this system, the reflected power measured for each condition is below the detection limit of the measuring probe and hence the reflected power is considered equal to zero. A more detailed description of the microwave set-up can be found in Ref. [34].

2.2. Mechanisms for CO_2 dissociation and product analyses

The dissociation of a CO_2 molecule is represented by the following global reaction [10]:

$$CO_2 \rightarrow CO + \frac{1}{2}O_2, \quad \Delta H = 2.9 \text{eV/molecule} \tag{1}$$
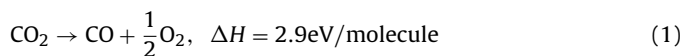
The following parameters describe the dissociation efficiency in the present study. By definition [10], the energy efficiency η of a dissociation process is given by:

$$\eta_{CO_2} = \frac{\Delta H}{E_{CO}} \tag{2}$$

where ΔH is the dissociation enthalpy of the global reaction [Eq. (1)], i.e. 2.9 eV/molecule, and E_{CO} is the specific energy input per molecule, i.e. the actual energy supplied to produce one CO molecule. The specific energy input per molecule, E_{CO}, is given by the ratio of the discharge power to the gas flow rate through the discharge volume and is measured in eV per molecule.

The composition of the post-discharge is analyzed by using a gas chromatograph (GC) (Bruker) equipped with a carbon molecular sieve column and a molecular sieve 5A column in series and connected to a thermal conductivity detector, which allowed a determination of the concentrations of O_2, CO and CO_2.

The conversion of CO_2 is calculated by comparing the GC CO_2 peak area before and after plasma processing. The conversion efficiency of CO_2 is calculated based on the following ratio:

$$CO_2 \text{ Conversion efficiency} (\%) = \frac{\text{moles of } CO_2 \text{ converted}}{\text{moles of } CO_2 \text{ in feed}}$$
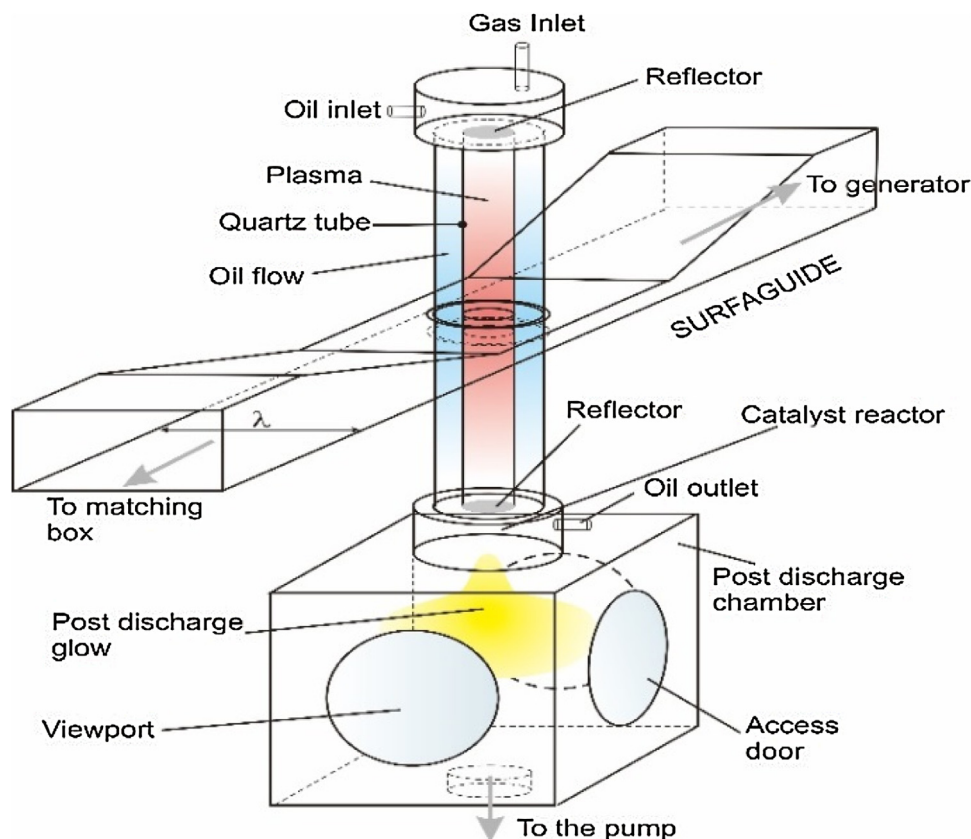$$\times 100\% \tag{3}$$

Fig. 1. Schematic representation of surface-wave microwave set-up.
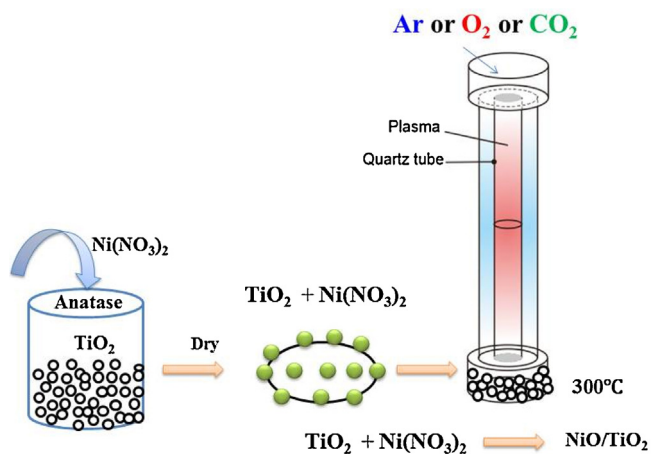

Fig. 2. Schematic representation of catalyst preparation by impregnation and plasma treatment methods.

2.3. Catalyst preparation

Catalysts with 10 wt.% NiO supported on TiO_2 pellets were prepared by combination of impregnation and plasma treatment methods (Fig. 2). The precursor was nickel nitrate hexahydrate $Ni(NO_3)_2 \cdot 6H_2O$ (Merck). Pellets (6 mm diameter and 1 mm thick) made from pure anatase powder (Sigma-Aldrich) were used as a catalyst support. The TiO_2 support was impregnated with the aqueous solution of $Ni(NO_3)_2 \cdot 6H_2O$ for 24 h and dried at 100 °C in air for 12 h. Plasma, induced in three different gases (O_2, Ar, CO_2), is used to treat the impregnated TiO_2 support with nickel nitrate in order to decompose the nickel nitrate and form NiO/TiO_2 catalyst. Hence, plasma treatment replaces the conventional calcination in the catalyst preparation process. Plasma processing was continued on for 40 min at a constant temperature of 300 °C.

The plasma operating parameters (applied power, pressure and gas flow rate) control the temperature in the catalytic reactor. Specific operating parameters were chosen for each investigated gas in order to keep the temperature in the catalytic reactor, constant at 300 °C. The flow rate was in the range of 2–4 slm, pressure ranged between 1330 and 2670 Pa (10–20 Torr) and the applied power for the three types of plasmas was set to 1 kW. The gas temperature in the catalytic reactor was measured by a thermocouple. Thermo gravimetric analysis (not presented here) showed that nickel nitrate, $Ni(NO_3)_2$, was completely decomposed above 290 °C. The three types of catalysts prepared by different gas plasmas are denoted in the following text as NiO/TiO_2 (O_2), NiO/TiO_2 (Ar) and NiO/TiO_2 (CO_2), respectively, for catalysts treated with pure O_2, pure Ar, or pure CO_2 discharge. In addition, we also investigated the activity of the TiO_2 support modified by Ar plasma. Therefore, pure TiO_2 pellets were pre-treated with an Ar plasma and denoted as TiO_2 (Ar), according to the same procedure. For CO_2 decomposition in the plasma-catalytic reactor, 8 g of the catalysts were used for each experiment. The operating conditions for the plasma-catalytic CO_2 decomposition are given above in Section 2.1.

2.4. Characterization of the catalysts

The following techniques and methods were used to characterize the catalysts before introduction in the plasma-catalytic reactor for CO_2 dissociation.

The surface area of the catalyst was determined by nitrogen adsorption at a temperature of 77 K with BET analysis.

Analysis of the crystalline structure of the catalyst was conducted by XRD in a Bruker advance X-ray diffractometer (40 kV,

40 mA) using a Cu Kα (0.154 nm) at a scanning rate of $2°$/min from $20°$ to $90°$.

TEM images were used to obtain the information about the sizes and morphology. For the TEM measurement, the catalyst samples were prepared by ultra-sonication in ethanol, followed by drop casting of the resultant suspension onto a carbon-coated copper grid.

The Raman spectra of the catalysts were recorded using a Raman spectrometer (Bruker) under ambient conditions, using a 532 nm argon ion laser as the excitation source. The spectra resolution was $0.1\,cm^{-1}$ and laser power was 2 mW. The Raman spectroscopy was used to detect defects in the crystal lattice.

UV–vis diffuse reflectance spectra were carried out by a UV–vis spectrometer (Cary) using $BaSO_4$ as a background at a resolution of $1\,cm^{-1}$. It was used for measurements of the bandgap energy and the absorbance of ultraviolet light as a function of the wavelength.

3. Results and discussion

3.1. Phase structure and morphology

The X-ray powder diffraction patterns of the different TiO_2 supported NiO catalysts, TiO_2 (Ar), and TiO_2 (anatase) support are presented in Fig. 3. The diffraction peaks located at 25.3, 37, 37.8, 38.5, 48.0, 54.0, 55.1, 62.7 and $68.8°$ correspond, respectively, to $(1\,0\,1)$, $(1\,0\,3)$, $(0\,0\,4)$, $(1\,1\,2)$, $(2\,0\,0)$, $(1\,0\,5)$, $(2\,1\,1)$, $(2\,0\,4)$ and $(2\,2\,0)$ planes of the anatase phase (JCPDS 21–1272) in TiO_2. It can be observed that, the peaks which can be ascribed to the tetragonal anatase phase of TiO_2 appear for all samples. No diffraction peaks corresponding to NiO($2\theta = 37$, 44.3, $62.9°$) could be detected, suggesting that Ni species are highly dispersed on the surface of TiO_2 support, producing various surface Ni or NiO species and clusters, or some Ni ions may be incorporated into the TiO_2 lattice [43]. Table 1 gives the lattice parameters (lattice constants a and c), the crystallite size and the BET area for the TiO_2 supported NiO catalysts, TiO_2 (Ar), and pure TiO_2 supports. The crystallite size of the catalyst was estimated from the XRD patterns according to the Scherrer's
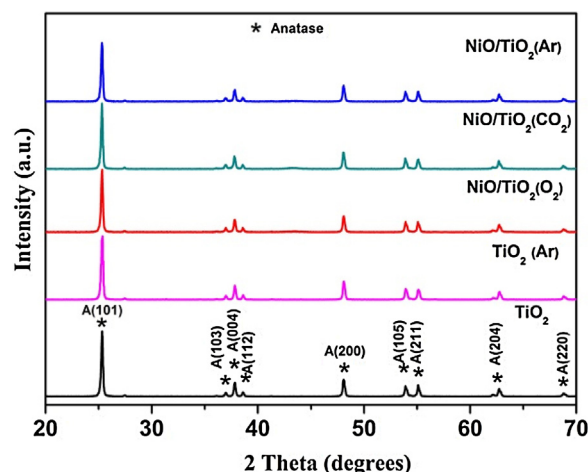
Fig. 3. XRD patterns of pure TiO_2 (anatase) support, TiO_2 (Ar), and NiO/TiO_2 (X) catalysts, prepared by different gas discharges X, where X can be Ar, CO_2, or O_2. The peaks, associated with the anatase phase and denoted with * in the XRD pattern of the pure TiO_2 (anatase) support, are observed with the same intensity in all samples.

equation. Similar crystallite sizes (around 46 nm) were observed for pure TiO_2 support, TiO_2 (Ar) and the NiO/TiO_2 catalysts prepared by plasma. The TEM images confirmed that indeed the 3 investigated catalysts and the support have similar crystallite sizes around 50 nm (see below)

Comparison of the lattice values for pure TiO_2 (anatase) with the NiO/TiO_2 catalysts (see Table 1) shows that the addition of NiO has little effect on the constant a while the lattice constant c shows a slight increase upon NiO loading and the largest change is observed for NiO/TiO_2 (Ar) catalyst. Since the ionic radius of Ni^{2+} (0.83 Å) is larger than that of Ti^{4+} (0.75 Å) [44], the observed TiO_2 lattice expansion might be an indication that a few Ni^{2+} ions substitute the Ti^{4+} ions [45]. The Raman spectra and UV–vis analysis (see next sub-sections) confirm the distortion of the TiO_2 structure by Ni^{2+}.
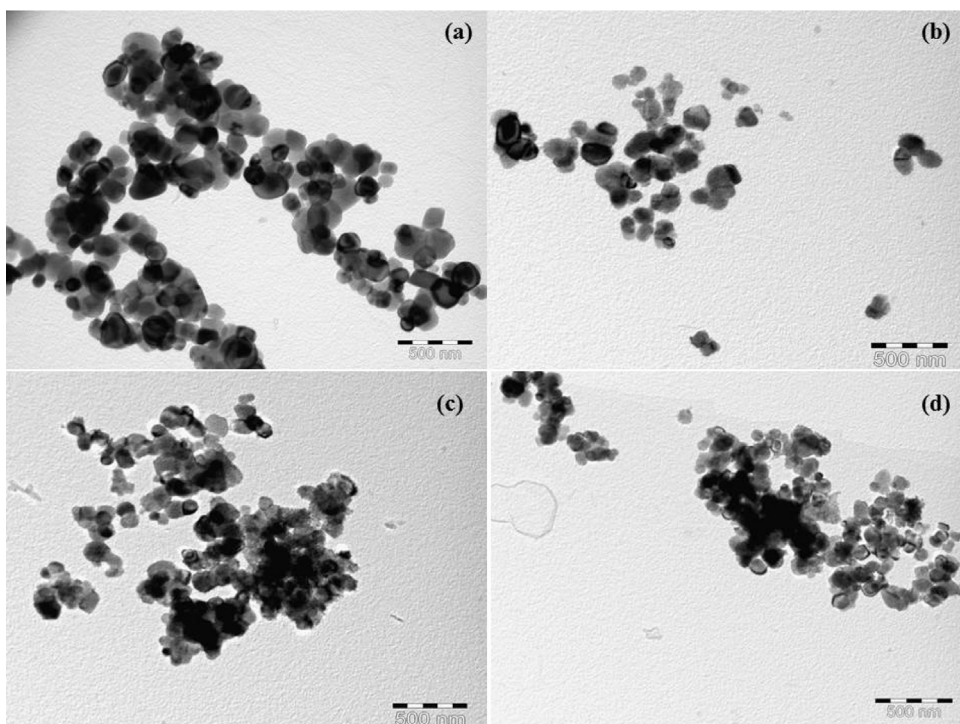
Fig. 4. TEM micrographs of (a) TiO_2, (b) NiO/TiO_2 (O_2), (c) NiO/TiO_2 (CO_2), and (d) NiO/TiO_2 (Ar).

Table 1
Properties of TiO$_2$ supported NiO catalysts treated by different plasma, TiO$_2$ (Ar), and pure TiO$_2$.

Catalysts	Lattice parameters		Crystallite size (nm)	BET surface area (m^2/g)
	a (Å)	c (Å)		
TiO$_2$ (anatase)	3.779	9.524	47	12
TiO$_2$ (Ar)	3.779	9.526	45	12
NiO/TiO$_2$(O$_2$)	3.780	9.541	46	15
NiO/TiO$_2$ (CO$_2$)	3.781	9.550	46	19
NiO/TiO$_2$ (Ar)	3.780	9.555	46	19
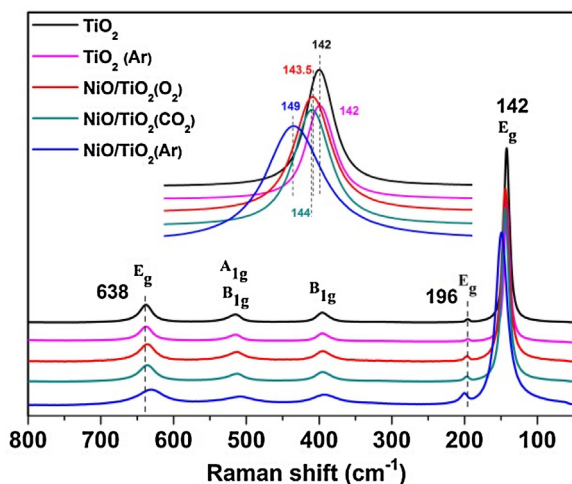
Fig. 5. Raman spectra of TiO$_2$ supported NiO catalysts, TiO$_2$ (Ar), and pure TiO$_2$ support. The enlarged view of the intense E$_g$ peak is shown in the inset of the figure.

An increase in BET surface area with the addition of NiO was measured (see Table 1). Similarly, An increase of the BET surface area when Ni is loaded to TiO$_2$ (anatase) photocatalyst was found by other authors [46]. However, the increase is relatively small for the catalyst pre-treated with O$_2$ plasma. The BET surface areas of NiO/TiO$_2$ (CO$_2$) and NiO/TiO$_2$ (Ar) are similar.

The analysis of the TiO$_2$ (Ar) data presented in Fig. 3 and Table 1 shows that Ar plasma pre-treatment does not change the TiO$_2$ crystalline structure, crystallite size and surface area.

TEM analysis was also performed on the different catalysts, in order to determine the particle sizes of NiO/TiO$_2$ (O$_2$), NiO/TiO$_2$ (Ar), and NiO/TiO$_2$ (CO$_2$) catalysts (Fig. 4a–d). The particle sizes and morphologies of the NiO/TiO$_2$ catalysts treated by different gas plasmas are very similar. These results show that the impregnation process and the different plasma treatments have little effect on the supported catalyst morphology.

3.2. Raman analysis

In order to determine the influence of different plasma, used for the catalyst preparation, on bonds present in the catalyst, Raman spectra of the catalysts were analyzed. Fig. 5 presents the Raman spectra of NiO/TiO$_2$ catalysts, TiO$_2$ (Ar), and pure TiO$_2$ support. Anatase TiO$_2$ has a tetragonal structure, and its unit cell is composed by two primitive cells, each with two TiO$_2$ units. It has six Raman (A$_{1g}$ + 2B$_{1g}$ + 3E$_g$) and three infra-red (IR) (A$_{2u}$ + 2E$_u$) active modes [47–49]. The strongest Raman band in pure TiO$_2$ (anatase) appears at 142 cm^{-1} corresponding to a E$_g$ mode (Fig. 5). The two other E$_g$ bands have lower intensity at 196 and 638 cm^{-1}. The doublet band at 515 cm^{-1} is assigned to A$_{1g}$ and B$_{1g}$ modes. The band appearing at 396 cm^{-1} belongs to B$_{1g}$ mode [47–49]. The E$_g$ peaks are associated with the symmetric stretching vibration of O—Ti—O in TiO$_2$. This mode is very sensitive to local oxygen coordination surrounding the metal ion [50,51]. The inset figure demonstrates

that the Raman 142 cm^{-1} peak of NiO/TiO$_2$ catalysts is blue-shifted (shifted to higher wavenumbers) and asymmetric broadened relatively to pure TiO$_2$. The 196 cm^{-1} peak also shows a blue shift, while the 638 cm^{-1} peak is red-shifted (shifted to lower wavenumbers). No shifts are observed for E$_g$ mode peaks in TiO$_2$ (Ar) spectrum relatively to the pure TiO$_2$ spectrum.

It has been reported that oxygen vacancies have a strong effect on the Raman spectrum of TiO$_2$ (i.e., broadening and shifting of Raman peaks, especially the peaks corresponding to the E$_g$ modes) [52–54]. In conjunction with XRD results, we conclude that indeed there is a distortion of the local structure of TiO$_2$ by doping with Ni^{2+} in the investigated NiO/TiO$_2$ catalysts. Each Ni^{2+} which substitutes a Ti^{4+} ion generates an oxygen vacancy to maintain charge neutrality. The disturbance of the Ti—O—Ti bonds and the new Ni-O bonds affect the Raman active modes and results in the broadening and shifting of the peaks. Researchers reported that crystallite size also affects the Raman spectrum [55,56]. However, the XRD and TEM results showed that the crystallite sizes of NiO/TiO$_2$ catalysts treated by different plasmas are similar to the crystallite size of pure TiO$_2$ (see Table 1). Therefore, oxygen vacancies are probably mainly responsible for the blue and red shifting and widening of the Raman peaks corresponding to E$_g$ modes. As it is noted from Fig. 5, the largest shift occurs for the Ar plasma treated NiO/TiO$_2$ catalyst. This indicates that the Ar plasma treatment leads to higher concentration of oxygen vacancies in presence of NiO.

Finally, it is important to report here that no carbon deposition was observed on the catalyst or the support after the plasma conversion of pure CO$_2$. No carbon peaks (D-band and G-band) were observed in the Raman spectrum of the used catalyst.

3.3. UV–vis analysis

The absorption spectra of pure TiO$_2$ support, TiO$_2$ (Ar) and of the catalysts treated by different plasmas are presented in Fig. 6 (a). Red shift is observed in the NiO/TiO$_2$ spectra, while there is no change in the TiO$_2$ (Ar) spectrum compared to the spectrum of pure TiO$_2$. The largest red shift occurs for the Ar plasma treated NiO/TiO$_2$ catalyst. This change in optical absorption was attributed to the formation of defect centers generated by the substitution of Ni^{2+} on the Ti^{4+} sites in the TiO$_2$ crystal structure [57]. Liu et al. [58] reported that the red shift resulted from the formation of surface oxygen vacancies. The shift was attributed to the overlap of the 3d level of the conduction band in Ti^{4+} with the d level of Ni^{2+} resulting in charge transfer transition between the electrons in the d level of Ni^{2+} and the conduction band of TiO$_2$ [59]. Based on the investigations reported in the literature [57–59] and the difference in the red shift observed in Fig. 6 (a) we might conclude that Ar plasma treatment forms the highest concentration of oxygen vacancies by substituting Ti^{4+} by Ni^{2+} in the anatase lattice. We suggest that, the catalyst prepared by one of the oxygen atom-containing plasmas (O$_2$ or CO$_2$) forms mainly NiO structures on TiO$_2$ support and relatively few Ni^{2+} ions are incorporated into the TiO$_2$ lattice, hence producing low or negligible oxygen vacancy concentration.
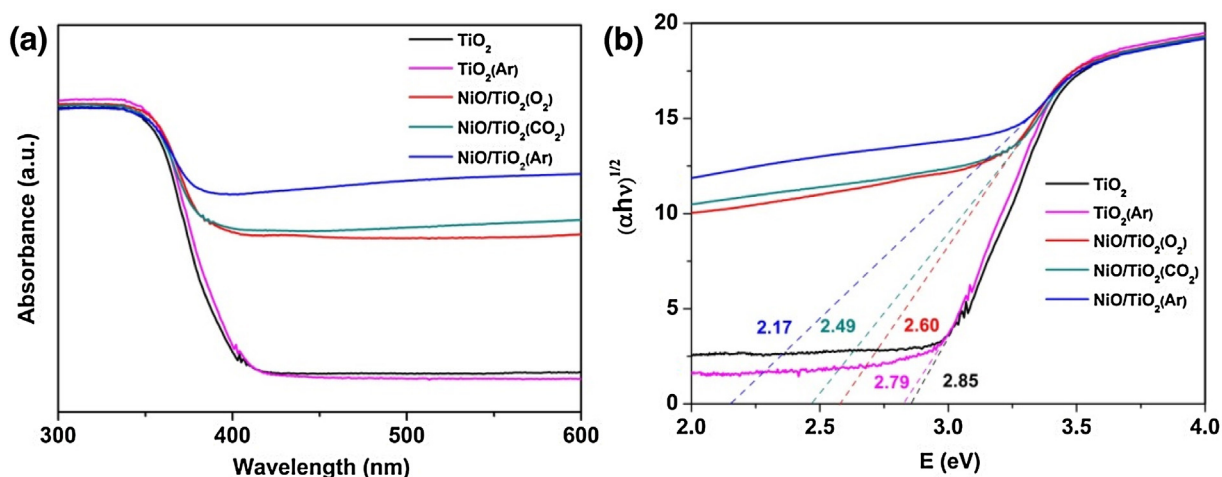
Fig. 6. UV–vis diffuse reflectance spectra (a) and the optical absorption edges (b) of TiO_2 supported NiO catalysts, TiO_2 (Ar) and pure TiO_2.

In order to study further the doping effect on the catalyst optical properties, the bandgap energy E_{bg} was calculated by using the following relation

$$(\alpha h\nu)^n = k(h\nu - E_{bg}) \qquad (4)$$

where α is the absorption coefficient, $h\nu$ is the absorption energy, n is 1/2 for a direct transition, and k is a constant [60].

Fig. 6 (b) shows the variation of $(\alpha h\nu)^{1/2}$ calculated from the optical absorption spectrum with the energy of the irradiation light. The intersection between the tangent at the inflexion point and the x-axis gives the bandgap energy value E_{bg} (Fig. 6(b)). The calculated E_{bg} obtained by this method are 2.17, 2.49 2.60, 2.79 and 2.85 eV for NiO/TiO_2 (Ar), NiO/TiO_2 (CO_2), NiO/TiO_2 (O_2), TiO_2 (Ar) and pure TiO_2, respectively. These results are consistent with the previous findings in the literature that an increase in the oxygen vacancy concentration leads to reduced bandgap energy for TiO_2 [61–65].

3.4. Plasma catalysis for CO_2 decomposition

The catalysts, prepared by the procedure described in Section 2.3, were used in the plasma reactor for CO_2 decomposition. The following operating parameters were used, as it is shown in the Section 2.1: pure CO_2 is supplied at flow rate of 2 slm, the mean input power is 1000 W at a pulse frequency of 1.67 kHz, which corresponds to a specific energy input of 6.95 eV/molecule, and the pressure in the post discharge is set to 1330 Pa (10 Torr). At the applied operating conditions, the measured catalyst temperature is above 200 °C. Comparison of CO_2 conversion and energy efficiencies in the surface-wave microwave discharge with and without catalysts as well as the effect of different gases used in plasma treatment of the catalyst are investigated and presented in Fig. 7. For each experiment 8 g of the catalysts (10 wt.% NiO/TiO_2) were used, corresponding to a space velocity of 15 L/(h.g). The space velocity denotes the quotient of the mass flow rate of the reactants divided by the mass of the catalyst in the reactor.

Both CO_2 conversion and energy efficiencies were significantly enhanced when NiO/TiO_2 (Ar) is used (Fig. 7). The CO_2 conversion and energy efficiencies increase almost by a factor of 2 from 23% to 42% and 9.6% to 17.2%, respectively, when compared with the results of the plasma only control experiment. On the other hand, NiO/TiO_2 (O_2) and NiO/TiO_2 (CO_2) catalysts did not affect significantly the CO_2 conversion and energy efficiencies. The CO_2 conversion and energy efficiencies are not modified by the presence of TiO_2 (Ar) support when compared to the plasma only experiment.
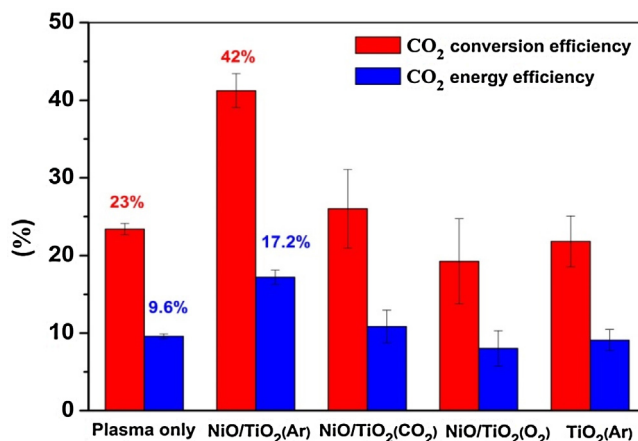

Fig. 7. CO_2 conversion and energy efficiencies, measured during the plasma-catalysis CO_2 dissociation, are shown for the NiO/TiO_2 catalysts prepared by plasma treatment with different gases (O_2, Ar, CO_2).

The CO_2 conversion efficiencies and the corresponding relative Raman shifts of the three E_g modes observed in NiO/TiO_2 (O_2, Ar, or CO_2) catalysts and in TiO_2 (Ar) (shown in Fig. 5), are plotted in Fig. 8. The larger relative Raman shift amplitude corresponds to the higher CO_2 conversion and energy efficiencies. This observation along with the UV–vis analysis indicates that the higher activity observed on Ar plasma-treated NiO/TiO_2 catalysts could be linked to the formation of surface oxygen vacancies.
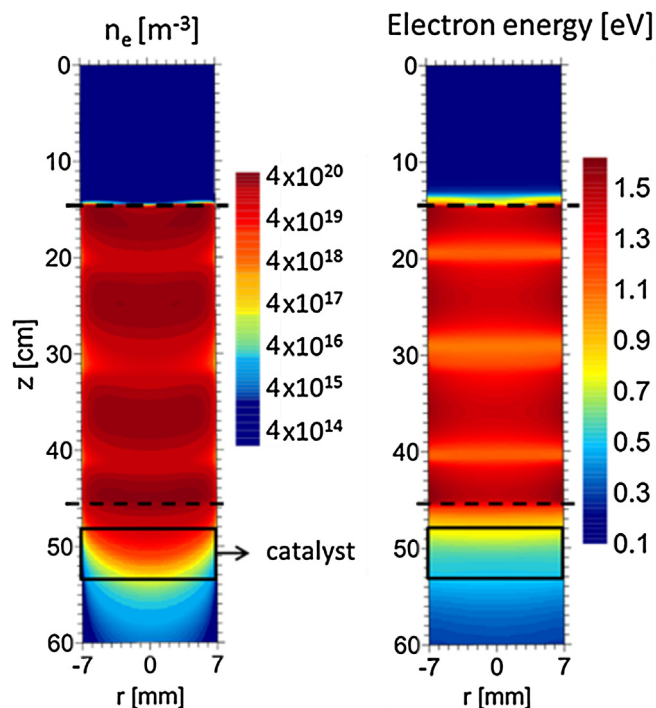
The dissociation of adsorbed CO_2 at oxygen vacancy defect on TiO_2 (110) surface was investigated by scanning tunneling microscope (STM) [66]. It was detected that the electron injection from the STM tip into the adsorbed CO_2 induces the dissociation of CO_2, i.e. *dissociative electron attachment* (DEA) was observed. The oxygen vacancy was found to be healed by the oxygen atom (noted below as bridging oxygen atom O_{br}) released during the dissociation process and the CO desorbed or moved from the reactive site [66]. It was demonstrated that the dissociation of CO_2 is a one-electron process with a threshold energy of 1.4 eV above the conduction-band minimum of TiO_2. The dissociation probability, determined by statistical analysis, was found to be dependent on the electron energy. The dissociation probability was calculated to be 0.02 at threshold electron energy of 1.7 eV (i.e. above that energy the injected electron started tunneling into the negative ion state of the absorbed CO_2) and it approaches 1 at electron energy of 2.2 eV [66].
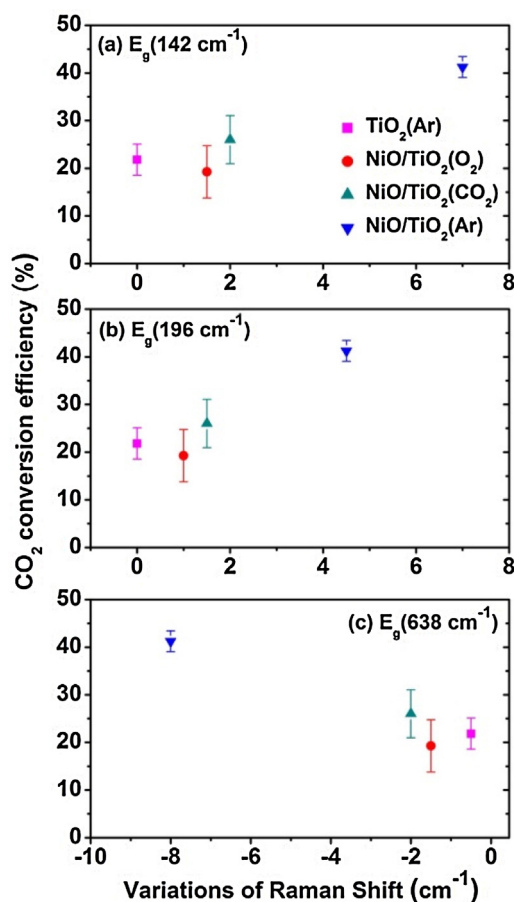
Fig. 8. CO_2 conversion efficiency related to the Raman shift in E_g modes measured in NiO/TiO_2 (O_2, Ar, or CO_2) and pure TiO_2 (Ar) spectra relatively to the spectrum of pure TiO_2 support (cf. with Fig. 5).

Fig. 9. 2-dimensional electron density and average electron energy profiles in Ar plasma calculated by fluid modelling at operating conditions in continuous regime (applied power 500W, flow rate 1 slm, pressure 30 Torr) similar to the operating conditions of experimental Ar plasma treatment of the catalyst in pulse regime. The gas is injected from the top, the dashed black lines show the two ends of the plasma tube, and the black rectangular represents schematically the catalyst, placed at around 3 cm below the plasma tube end (cf. Fig. 1).

Moreover, in recent years, it has been demonstrated that fabrication of oxygen-deficient surfaces is an important strategy for enhancing photocatalytic CO_2 dissociation [67]. In-situ diffuse reflectance infrared Fourier transform spectroscopy studies confirmed that the exposure of defective Rh/TiO_2-x [68] or $Cu(I)/TiO_{2-x}$ [69] surfaces to CO_2 rapidly led to generation of metastable CO_2^- bonded to Ti^{4+} even in the dark. The formation of $CO_2^- - Ti^{4+}$ suggests that the excess electrons trapped in Ti^{3+}/V_O sites migrate spontaneously to the adsorbed CO_2 and enhance the DEA dissociation into CO [67–69]. The DEA of CO_2 observed on the catalytic surface can happen also in the gas phase [10]. However, the maximum value of the DEA cross-section is low ($\sim 10^{-22}$ m^2) and the threshold energy of 5–10 eV [10,p. 267] is high compared to the threshold energy of 1.7 eV [66] for the DEA at the catalyst surface. Because of the large binding energy of the bridging oxygen [70] the DEA process for CO_2 occurs more easily for the CO_2 adsorbed at the TiO_2 defective surface than for CO_2 in the gas phase.

Based on the presented experimental results of the NiO/TiO_2 catalyst prepared by Ar plasma and the STM investigation by Lee et al. [66], we propose the following plasma-catalytic mechanism of CO_2 dissociation. The oxygen vacancies on the NiO/TiO_2 (Ar) catalyst surface provide sites for the adsorption of oxygen atoms from CO_2, i.e. CO_2 is more easily adsorbed at the defect surfaces compared to detect-free surfaces [67]. The energetic electrons supplied by the plasma (see below an example of the simulated electron energy and density profiles in Ar microwave plasma) induce the formation of the transient negative ion CO_2^-, which is dissociated to CO and O^- by the DEA process observed in

the STM investigation of Lee et al. [66]. Subsequently, CO desorbs or moves from the reactive site while the other O atom heals an oxygen vacancy and the excess electron is released [66,67].

In order to understand and control the microwave plasma, we investigated it by computational fluid dynamics. The model, developed in the modelling software Plasimo [71], and results from the simulated plasma characteristics and their dependence on operating parameters, as well as comparison with experimental measurements is the topic of another paper [72]. Initially, the model was developed for Ar plasma. The results for the electron density and energy at operating conditions in continuous regime close to the operating conditions for Ar plasma treatment of catalysts in pulsed regime are shown in Fig. 9. The position of the catalyst at around 3 cm below the plasma tube is shown. It is clearly observed that at the considered operating conditions, plasma extends and reaches the catalyst. The striation patterns in the profiles presented in Fig. 9 can be explained as follows. Surface waves were obtained only as slow waves, i.e. the phase velocity is smaller than the light speed c in the surrounding dielectric with a relative permittivity ε_r [73]. The dielectric permittivity of quartz is close to 4, hence the wave phase velocity $c/\sqrt{\varepsilon_r}$ is 1.5×10^8 m/s. Thus the wavelength is calculated to be around 16 cm for an applied frequency of 915 MHz. The metal rings at the plasma tube (31 cm in length) ends confine the electromagnetic field and the surface waves are reflected. Hence, standing waves are formed and local maxima along the tube length are formed at a distance close to a half wavelength. The distance between the maxima is not a constant due to the wave-plasma interaction and the strong gas flow velocity. The calculated electron number density at the position of the catalyst reactor surface is above 10^{19} m^{-3}. The average electron energy at the same position is around 0.9 eV. Experimental
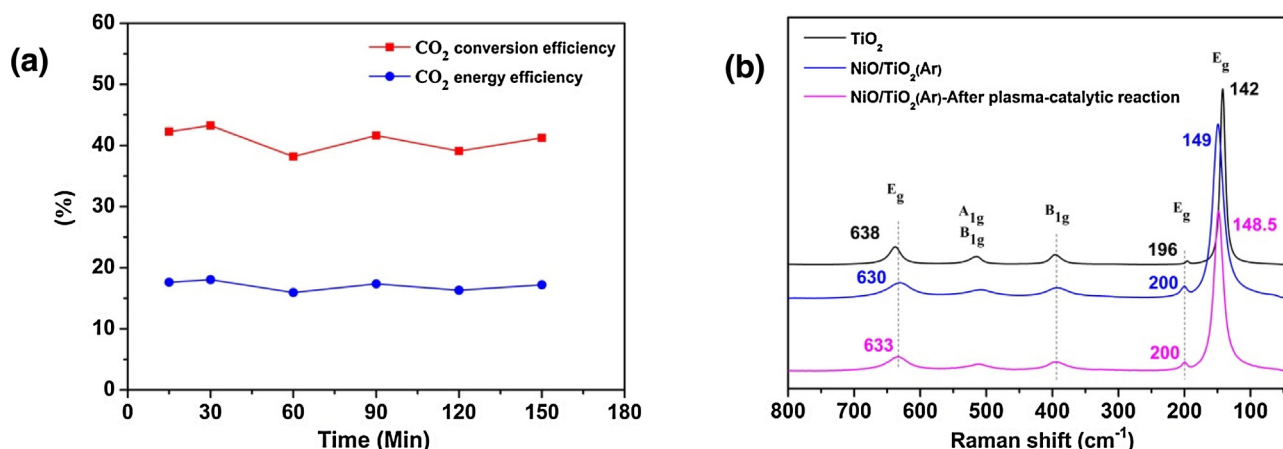
Fig. 10. CO_2 conversion and energy efficiencies as a function of time (a) for NiO/TiO$_2$ (Ar). The Raman spectra (b) of the NiO/TiO$_2$ (Ar) before and after its use for 150 min compared to the Raman spectrum of pure TiO$_2$.

measurements of electron density or energy at the catalyst position were not possible due to solid metallic parts surrounding the plasma tube end and the catalytic reactor. Therefore, the experimentally measured gas temperature in the catalytic reactor was an indication of plasma reaching the catalyst surface. The temperature during the Ar plasma catalyst pre-treatment was measured around 300 °C (see Section 2.3), and during CO_2 dissociation was measured to be above 200 °C in the catalytic reactor (note that the cooling system keeps the plasma tube walls at 5 °C). High gas temperatures on the order of 300–500 °C were also calculated in the catalytic reactor by the model for the conditions presented in Fig. 9.

The CO_2 conversion and energy efficiencies remained more or less constant over time at least for 150 min of continuous operation [Fig. 10(a)]. The activity of the NiO/TiO$_2$ (Ar) catalyst remains constant which means that the oxygen vacancies are regenerated continuously. Fig. 10(b) presents the Raman spectra of the NiO/TiO$_2$ (Ar) before and after its use for 150 min in the reactor. The Raman spectrum of pure TiO$_2$ is also shown for comparison. The Raman shifts in E_g modes confirm the presence of oxygen vacancies in the used catalyst, indicating the NiO/TiO$_2$ (Ar) catalyst regeneration. In photocatalytic CO_2 reduction it is suggested that photo-illumination forms surface oxygen vacancies in a way that the surface oxygen atoms are oxidized to O_2 by photo-generated holes [67]. The O_2 molecule then is easily desorbed producing an oxygen vacancy. In the present investigation we may expect that there is ultra-violet (UV) light emitted from the CO_2 plasma, which might photo-activate the pure TiO$_2$. However, when a pure TiO$_2$ (Ar) support was used in the catalytic reactor, no difference in the CO_2 conversion rates compared to plasma only assisted conversion was found (see Fig. 7). Kim et al. [74] have shown that plasma does not have enough UV photon flux to photo-excite a photocatalyst. Although it is true that plasma can generate UV light in an air-like gas mixture, its photon flux is too low to make any significant contribution to the catalytic reaction. The measurement of the UV flux in air revealed that it is only in the order of several μW cm^{-2}, which is about three orders of magnitudes less than that of outdoor UV flux in daytime ($\sim$mW cm^{-2})[75]. Mei and Huang et al. confirmed the weaker UV intensity in a DBD reactor, compared to a UV lamp [76,77]. Based on the above results, the photocatalytic properties could not be activated only by plasma irradiation or it plays only a minor role due to its low intensity compared to that emitted by an UV lamp. Hence, the observed regeneration could not be explained by the possible photocatalytic oxidation of the TiO$_2$ surface oxide atoms to O_2.

Another possible mechanism is the recombination on oxide surfaces of the adsorbed oxygen atom with gaseous oxygen atom [78–80].

$$O_{ads} + O(g) \rightarrow O_2(g) \tag{6}$$

The activation energy for the recombination of oxygen atoms on different oxide surfaces is low, in the range 0.043–0.48 eV, and, in general, the recombination coefficient increases with increasing surface temperature [78,80]. The presence of the atomic O peaks (at 777 nm ($3p^5P$–$3s^5S$), and 844 nm ($3p^3P$–$3s^3S$)) in the emission spectrum of CO_2 microwave discharge was clearly detected and reported in our previous study [34]. The plasma supplies O atoms not only in ground state but also in excited state, as well as other energetic species [10], which bring additional energy to the catalyst surface and thus may enhance the recombination process. In the CO_2 plasma-assisted dissociation, the step-by-step vibrational excitation is very important because of the lowest threshold energy of 5.5 eV for CO_2 splitting, which is exactly the energy needed for breaking the OC=O bond [10]. The reaction produces oxygen atom in the electronically ground state $O(^3P)$ [10]. The straightforward adiabatic dissociation of the vibrationally excited CO_2 requires higher energy, more than 7 eV, and produces electronically excited oxygen atom $O(^3D)$ [10]. Because of the higher threshold energy, the probability for the latter process is very low, and hence the produced oxygen atoms are expected to be mainly in ground state. However, there are other mechanisms for excitation of the oxygen atoms by electron impact, for example. Currently, we could not find sufficient data for the fluxes of different species in CO_2 plasma. Therefore, further experimental measurements and modelling of CO_2 plasma chemistry is expected to clarify the catalyst regeneration process.

We investigated the catalyst activity over time for 150 min also for the catalysts prepared by CO_2 or O_2 plasma and we found that the CO_2 conversion and energy efficiencies do not change with time (not presented here). Hence, we conclude that new oxygen vacancies are not created through the plasma-catalyst CO_2 dissociation at the conditions under study and the steady-state concentration of oxygen vacancies depends on their initial concentration.

In summary, we proposed that the plasma-catalyst assisted CO_2 dissociation at the catalyst surface can be explained by the following steps:

1) CO_2 adsorption at V_O (V_O are formed during Ar plasma pre-treatment of the NiO/TiO$_2$ catalyst. The presence of nickel is necessary to have the activity of the vacancy in the reaction.)

2) $CO_2 + V_O \xrightarrow{\text{energetic } e^- \text{ sipplied by plasma}} CO + O^- \rightarrow CO(g) + O_{br} + e^-$ (the energy threshold of the dissociative electron attachment is reduced at the catalyst surface to 2 eV, compared with the energy threshold of 5–10 eV in gas phase)

3) $O(g) + O_{br} \rightarrow O_2 (g) + V_O$ (Atomic O supplied by the discharge recombines with the adsorbed, bridging O atoms, regenerating the oxygen vacancy).

Hence, a synergy between the plasma and the NiO/TiO$_2$ (Ar) catalyst leads to significantly improved CO$_2$ conversion and energy efficiencies compared to the plasma only process (see Fig. 7), regenerating the catalyst at the same time. While the main gas phase dissociation mechanism in the (non-thermal) plasma is the stepwise vibrational excitation of CO$_2$ molecule [2], at the catalyst surface with oxygen vacancies it is dissociative electron attachment.

4. Conclusions

The conversion of CO$_2$ in a microwave plasma system in the presence of TiO$_2$ supported NiO catalysts pre-treated by plasma was carried out. Three different plasma compositions (O$_2$, Ar, CO$_2$) were considered to prepare the catalysts. The influence of the different gas plasma pre-treatments on the chemical and physical properties of the catalysts were studied by X-ray diffraction, nitrogen adsorption–desorption (BET analysis), TEM, Raman spectroscopy and UV–vis diffuse reflectance spectra techniques. The analyses show formation of oxygen vacancies especially in the NiO/TiO$_2$ catalyst treated by the Ar plasma. The pure TiO$_2$ support and the TiO$_2$ support pre-treated with Ar plasma were also investigated. No influence of Ar plasma pre-treatment was found on the TiO$_2$ support crystalline structure and active surface area, as well as, on defect formation. Therefore, an important condition for formation of oxygen vacancies in Ar (non-oxygen containing gas) plasma pre-treated catalyst is the presence of Ni or NiO.

The influence of the catalysts on the CO$_2$ conversion and energy efficiencies was evaluated. The highest activity was observed for NiO/TiO$_2$ catalyst prepared by Ar plasma. The conversion and energy efficiencies increased almost by a factor of 2 in plasma—NiO/TiO$_2$ (Ar) catalyst system compared to the plasma only assisted dissociation. This enhancement could be attributed to the formation of oxygen vacancies on the catalyst surface. The oxygen vacancies provide sites for the adsorption of oxygen atoms from CO$_2$. The energetic electrons supplied by the plasma enhance the dissociative electron attachment of CO$_2$ at the surface. Subsequently, CO desorbs or moves from the reactive site while the other O (bridging) atom heals the oxygen vacancy.

In addition, we have observed a relatively constant activity of the NiO/TiO$_2$ (Ar) catalyst, i.e. there is a mechanism for the catalyst regeneration. We suggest that the oxygen vacancies are regenerated via recombination of the bridging O atoms and gaseous O atoms supplied by plasma. In conclusion, we propose a mechanism that explains the observed plasma-catalyst synergy, which has led to improved CO$_2$ conversion and energy efficiencies by CO$_2$ dissociation both in the plasma and on the catalyst surface, when compared to the plasma only experiment.

Acknowledgments

References

[1] S. Rayne, Nat. Preced. (2008), http://dx.doi.org/10.1038/npre.2008.1741.1.
[2] Y. Nigara, B. Cales, Chem. Soc. Jpn. 59 (1986) 1997–2002.
[3] B. Pan, S. Luo, W. Su, X. Wang, Appl. Catal. B 168–169 (2015) 458–464.
[4] B. Hu, C. Guild, S.L. Suib, J. CO$_2$ Util. 1 (2013) 18–27.
[5] M. Hussaina, P. Akhter, G. Saracco, N. Russo, Appl. Catal. B 170–171 (2015) 53–65.
[6] E.B. Stechel, J.E. Miller, J. CO$_2$ Util. 1 (2013) 28–36.
[7] S.C. Roy, O.K. Varghese, M. Paulose, C.A. Grimes, ACS Nano 4 (2010) 1259–1278.
[8] C. Graves, S.D. Ebbesen, M. Mogensen, K.S. Lackner, Renewable Sustainable Energy Rev. 15 (2011) 1–23.
[9] C. Liu, G. Xu, T. Wang, Fuel Process. Technol. 58 (1999) 119–134.
[10] A. Fridman, Plasma Chemistry, University Press, Cambridge, 2008.
[11] Q. Yu, M. Kong, T. Liu, J. Fei, X. Zheng, Plasma Chem. Plasma Process. 32 (2012) 153–163.
[12] S. Paulussen, B. Verheyde, T. Xin, C.D. Bie, T. Martens, D. Petrovic, A. Bogaerts, B. Sels, Plasma Sources Sci. Technol. 19 (2010) 034015.
[13] R. Aerts, W. Somers, A. Bogaerts, ChemSusChem 8 (2015) 702–716.
[14] R. Li, Y. Yamaguchi, S. Yin, Q. Yang, T. Sato, Solid State Ion. 172 (2004) 235–238.
[15] S.L. Brock, M. Marquez, S.L. Suib, Y. Hayashi, H. Matsumoto, J. Catal. 180 (1998) 225–233.
[16] R. Li, Q. Tang, S. Yin, T. Sato, Fuel Process. Technol. 87 (2006) 617–622.
[17] R. Li, Q. Tang, S. Yin, T. Sato, Appl. Phys. Lett. 90 (2007) 131502.
[18] G. Horvath, J.D. Skalny, N.J. Mason, J. Phys. D: Appl. Phys. 41 (2008) 225207.
[19] L.F. Spencer, A.D. Gallimore, Plasma Sources Sci. Technol. 22 (2013) 015019.
[20] J.Y. Wang, G.G. Xia, A. Huang, S.L. Suib, Y. Hayashi, H. Matsumoto, J. Catal. 185 (1999) 152–159.
[21] A.P.H. Goede, W.A. Bongers, M.F. Graswinckel, M.C.M. Richard van de Sanden, M. Leins, J. Kopecki, A. Schulz, M. Walker, EPJ Web Conf. 79 (2014) 01005, http://dx.doi.org/10.1051/epjconf/20147901005.
[22] S. Mori, A. Yamamoto, M. Suzuki, Plasma Sources Sci. Technol. 15 (2006) 609–613.
[23] X. Duan, Y. Li, W. Li, B. Wang, Greenh. Gas Sci. Technol. 5 (2014) 131–140.
[24] M. Kano, G. Satoh, S. Iizuka, Plasma Chem. Plasma Process. 32 (2012) 177–185.
[25] E. Jwa, S.B. Lee, H.W. Lee, Y.S. Mok, Fuel Process. Technol. 108 (2013) 89–93.
[26] B. Eliasson, U. Kogelschatz, B. Xue, L.M. Zhou, Ind. Eng. Chem. Res. 37 (1998) 3350–3357.
[27] M. Heintze, B. Pietruszka, Catal. Today 89 (2004) 21–25.
[28] J. Sentek, K. Krawczyk, M. Mlotek, M. Kalczewska, T. Kroker, T. Kolb, A. Schenk, K.H. Gericke, K. Schmidt-Szałowski, Appl. Catal. B 94 (2010) 19–26.
[29] H. Long, S. Shang, X. Tao, Y. Yin, X. Dai, Int. J. Hydrogen Energy 33 (2008) 5510–5515.
[30] A.J. Zhang, A.M. Zhu, J. Guo, Y. Xu, C. Shi, Chem. Eng. J. 156 (2010) 601–606.
[31] A.M. Ghorbanzadeh, R. Lotfalipour, S. Rezaei, Int. J. Hydrogen Energy 34 (2009) 293–298.
[32] H.J. Gallon, X. Tu, M.V. Twigg, J.C. Whitehead, Appl. Catal. B 106 (2011) 616–620.
[33] X. Tu, J.C. Whitehead, Appl. Catal. B 125 (2012) 439–448.
[34] G. Chen, T. Silva, V. Georgieva, T. Godfroid, N. Britun, R. Snyders, M.-P. Delplancke-Ogletree, Int. J. Hydrogen Energy 40 (2015) 3789–3796.
[35] S. Mahammadunnisa, L. Reddy, D. Ray, C. Subrahmanyam, J.C. Whitehead, Int. J. Greenh. Gas Control 16 (2013) 361–363.
[36] S. Futamura, H. Kabashima, Fuel Chem. Div. Prepr. 48 (2003) 266–267.
[37] S. Futamura, H. Kabashima, Stud. Surf. Sci. Catal. 153 (2004) 119–124.
[38] H.L. Chen, H.M. Lee, S.H. Chen, Y. Chao, M.B. Chang, Appl. Catal. B 85 (2008) 1–9.
[39] J. Van Durme, J. Dewulf, C. Leys, H. Van Langenhove, Appl. Catal. B 78 (2008) 324–333.
[40] M.B. Kizling, S.G. Järàs, Appl. Catal. A 147 (1996) 1–21.
[41] C. Liu, G.P. Vissokovb, B.W.L. Jang, Catal. Today 72 (2002) 173–184.
[42] C. Liu, J. Zou, K. Yu, D. Cheng, Y. Han, J. Zhan, C. Ratanatawanate, B.W.L. Jang, Pure Appl. Chem. 78 (2006) 1227–1238.
[43] G. Chen, Q. Li, Y. Wei, W. Fang, Y. Yang, Chin. J. Catal. 34 (2013) 322–329.
[44] R.D. Shannon, Acta Cryst. A 32 (1976) 751–767.
[45] M. Saraiva, V. Georgieva, S. Mahieu, K. Van Aeken, A. Bogaerts, D. Depla, J. Appl. Phys. 107 (2010) 034902.
[46] O. Ola, M.M. Maroto-valer, J. Catal. 309 (2014) 300–308.
[47] H. Berger, H. Tang, F. levy, J. Cryst. Growth 130 (1993) 108–112.
[48] J. Zhang, M. Li, Z. Feng, J. Chen, C. Li, J. Phys. Chem. B 110 (2006) 927–935.
[49] B. Choudhury, A. Choudhhury, Mater. Chem. Phys. 132 (2012) 1112–1118.
[50] F. Tian, Y. Zhang, J. Zhang, C. Pan, J. Phys. Chem. C 112 (2012) 7515–7519.
[51] H.Y. Lin, Y.Y. Chou, C.L. Cheng, Y.F. Chen, Opt. Express 15 (2007) 13832–13837.
[52] D. Bersani, P.P. Lottici, X.Z. Ding, Appl. Phy. Lett. 72 (1998) 73–75.
[53] B. Choudhury, Curr. Appl. Phys. 13 (2013) 1025–1031.
[54] J.C. Parker, R.W. Siegel, Appl. Phys. Lett. 57 (1990) 943–945.
[55] X. Xue, W. Ji, Z. Mao, H. Mao, Y. Wang, X. Wang, W. Ruan, B. Zhao, J.R. Lombardi, J. Phys. Chem. C 116 (2012) 8792–8797.
[56] A.L. Bassi, D. Cattaneo, V. Russo, C.E. Bottani, E. Bartoriri, T. Mazza, P. Pisen, P. Midani, F.O. Ernst, K. Wegner, S.E. Pratsinis, J. Appl. Phys. 98 (2005) 74305.

[57] M. Sahu, P. Biswas, Nanosci. Res. Lett. 6 (2011) 441–454.
[58] L. Liu, H. Zhao, J.M. Andino, Y. Li, ACS. Catal. 2 (2012) 1817–1828.
[59] L. Sim, K. Ng, S. Ibrahim, P. Saravanan, Int. J. Photoenergy 2013 (2013) 1–10.
[60] M. Yoon, M. Seo, C. Jeong, J.H. Kang, K.S. Jeon, Chem. Mater. 17 (2005) 6069.
[61] H. Liu, F. Zeng, Y. Lin, G. Wang, Feng Pan, Appl. Phys. Lett. 102 (2013) 181908.
[62] Y. Wang, F. Wang, Y. Chen, D. Zhang, B. Li, S. Kang, X. Li, L.C. Appl, Catalysis B 147 (2014) 602–609.
[63] B. Choudhury, M. Dey, A. Choudhury, Int. Nano Lett. 3 (2013) 25.
[64] S. Suib, New and Future Developments in Catalysis, Elsevier, Amsterdam, 2013.
[65] Y. Wang, R. Zhang, J. Li, L. Li, S. Lin, Nanoscale Res. Lett. 9 (2014) 46.
[66] J. Lee, D.C. Sorescu, X. Deng, J. Am. Chem. Soc. 133 (2011) 10066–10069.
[67] L. Liu, Y. Li, Aerosol. Air Qual. Res. 14 (2014) 453–469.
[68] J. Rasko, F. Solymosi, J. Phys. Chem. 98 (1994) 7147–7152.
[69] L. Liu, C. Zhao, Y. Li, J. Phys. Chem. C 116 (2012) 7904–7912.
[70] M.V. Ganduglia-Pirovano, A. Hofmann, J. Sauer. Surf. Sci. Rep. 62 (2007) 219.
[71] M. Jimenez-Diaz, A.D.E. Carbone, J. van. Dijk, J.J.A.M. van der. Mullen, J. Phys. D: Appl. Phys. 45 (2012) 335204.
[72] V. Georgieva, T. Silva, N. Britun, G. Chen, T. Godfroid, R. Snyders, M.-P. Delplancke-Ogletree, IX International Workshop on Microwave Discharges (MD-9) (2015).
[73] H. Schlüter, A. Shivarova, Phys. Rep. 443 (2007) 121–255.
[74] H.H. Kim, Y. Teramoto, N. Negishi, A. Ogata, Catal. Today. 256 (2015) 13–22.
[75] T. Sano, N. Negishi, E. Sakai, S. Matsuzawa, J. Mol. Catal. A: Chem. 245 (2006) 235–241.
[76] D. Mei, X. Zhu, C. Wu, B. Ashford, P.T. Williams, X. Tu, Appl. Catal. B 182 (2016) 525–532.
[77] H.B. Huang, D.Q. Ye, M.L. Fu, F.D. Feng, Plasma Chem. Plasma Proc. 27 (2007) 577–588.
[78] P.G. Dickens, M.B. Sutcliffe, Trans. Faraday Soc. 60 (1964) 1272–1285.
[79] P.J. Crane, P.G. Dickens, R.E. Thomas, Trans. Faraday Soc. 63 (1967) 693–700.
[80] V.L. Kovalev, A.A. Krupnov, M. Yu Pogosbekyan, L.P. Sukhanov, Acta Astronaut. 68 (2011) 686–690.